

Single-shot multispectral imaging through a thin scatterer: supplementary material

XIAOHAN LI, JOEL A. GREENBERG, AND MICHAEL E. GEHM*

Electronic and Computer Engineering Department, Duke University, 101 Science Drive, Durham, NC 27708, USA

*Corresponding author: michael.gehm@duke.edu

Published 9 July 2019

This document contains supplementary information to "Single-shot multispectral imaging through a thin scatterer," <https://doi.org/10.1364/OPTICA.6.000864>. We provide details and discussion related to our technique for performing multispectral imaging through a scatterer, including the experiment setup and components, calibration procedure and reconstruction algorithms. We also analyze the spectral resolution of the system and discuss the fundamental limitations of our system.

1. SYSTEM CONFIGURATIONS

The schematics for the experimental setups we used to generate objects with widely-separated and contiguous spectral bands are displayed in Figs. S1 (a) and (b), respectively. In both cases, we generate the color objects in a controlled and well-characterized way using a multi-step process starting with a broadband lamp (Newport 66921, 500W) with a spectral range from 200 to 2500 nm. The light then passes through an integrating sphere so that it is sufficiently spatially incoherent and static. While this approach sacrifices a significant amount of optical power, it has the advantage that we can create a broad range of interesting objects with complete knowledge about their spectral and spatial characteristics. Thus, we can perform quantitative comparisons between the ground truth and estimated objects.

For the objects with widely-separated spectra, the light then passes through a set of multi-bandpass spectral filters (Semrock AVOR-0012, NF03-658E-25, FF01-430/LP-25, FF01-745/SP-25, NF03-561E-25), which results in three spectral channels centered at 450, 550 and 650 nm with bandwidths of 11, 8.8 and 5.7 nm full width at half maximum (FWHM), respectively. The specific choice of wavelengths is arbitrary, and intended only to demonstrate the capabilities of the system to perform multi-spectral imaging over a broad spectral range. We define the color object (i.e., impose a specific weighting of each spectral component at each location) by passing the filtered light through a pair of spatial light modulators (SLMs): the first SLM (Holoeye LC2012) is placed between a pair of crossed polarizers and generates a high-contrast, spectrally-uniform object shape, whereas the second SLM (Pluto) imposes a spatio-spectrally varying modulation by virtue of its voltage-controlled wavelength-dependence. Finally, we place a machine vision lens (Computar TEC-55) 12 cm away from and focused on the second SLM in order to better fit the object within the ME field of view.

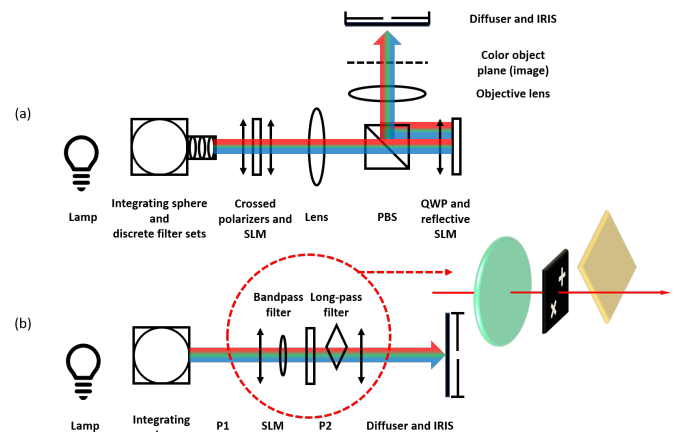


Fig. S1. Experiment setup for object generation. (a) Configuration of discrete spectral band object. (b) Configuration of continuous spectral band object.

For objects with contiguous spectra, we only keep the first SLM (LC 2012) and the crossed polarizers between the integrating sphere and the scattering media to generate the object (see Fig. S1 (b)). We eliminate the second SLM because its spectral response is largely unstructured over the contiguous spectral bands over which we focus (typically 50 - 100 nm). Removal of the second SLM simplifies the setup and significantly increases the signal power along the optical path. To control the spectral profile of the illumination, we use a band pass filter (Semrock FF01-545/55-25), which provides a continuous spectrum of 60 nm between 515 and 575 nm. We used an additional longpass filter (Thorlabs FGL550S - 2") to partially block some of the object space. In the object described in Fig. 5, for example, the plus sign has a spectrum that corresponds to the combination of the the filters and the letter "X" has the full spectrum of the bandpass filter.

2. SPECTRAL CORRELATION LENGTH

We characterize the speckle spectral decorrelation bandwidth of a our diffuser using our broadband lamp source in combination with a set of contiguous, 10 nm wide filters. We place each filter at the exit port of the integrating sphere one at a time and record the resulting speckle pattern. We then calculate the maximum correlation between the a particular spectral channel and all others. Figure S2 shows that the spectral correlation length of our diffuser is approximately 15 nm (at FWHM).

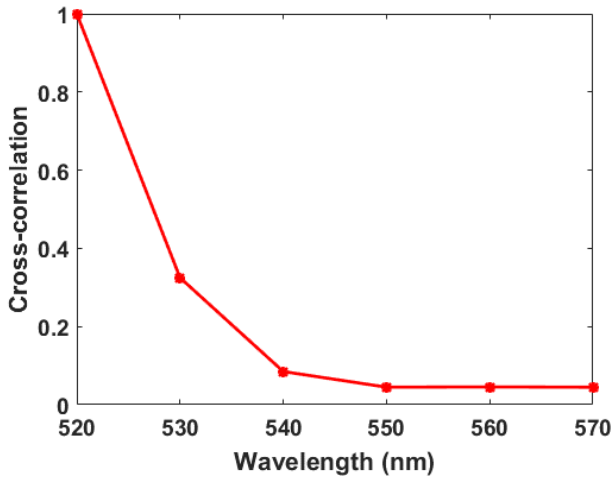


Fig. S2. Spectral correlation length Magnitude of the maximum speckle correlation for a 660 grit optical diffuser.

3. EXAMPLE SPECKLE PATTERNS

The speckle that we observe are well-developed and extend across multiple detector pixels. Figure S3 (a) shows an example of a multiplexed, coded speckle measurement for the contiguous, six-channel spectrum. The overall beam intensity can be seen in the circular structure, and a zoomed-in region (corresponding to the location of the black box) shows the low contrast, coded speckle grains. After demultiplexing the signal, we recover six separate speckle channels, which are shown in Fig. S3 (b) in full (and a small, zoomed-in patch in Fig. S3 (c)). It is clear that the recovered speckle from each channel are distinct and of higher contrast than the multiplexed, "broadband" speckle pattern.

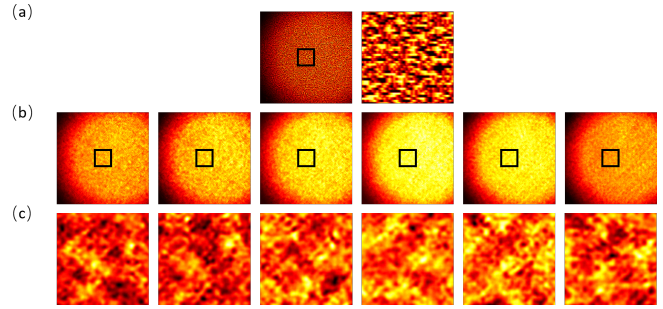


Fig. S3. Representative speckle measurements (a) Multi-multiplexed speckle measured using the widely-spaced six-channel spectrum (far away and zoomed in, where both speckle structure and coding structure are present). Recovered speckle patterns at each of the six spectral channels (b) for the full measurement and (c) for a zoomed-in region.

4. SCAN TIME CONSIDERATIONS

It is important to stress that the long exposure times used in most of the experiments arise because of the severe photon loss introduced by the optical components (integrating sphere, multiple spatial light modulators, polarizers, etc.) that were inserted in the system to create a controllable source object to facilitate quantitative performance comparison of our proposed method and that these components will not be present in any real-world application. Based on measured changes in the signal strength arising from these components, we anticipate reductions in the exposure time of up to 10^4 to 10^6 (suggesting ultimate exposure times of 2-200 ms). The resulting exposure times would be consistent with exposure times reported in other recent ME imaging results (which is to be expected as our coding technique introduces only a factor of 2x photon loss from the opaque region of the aperture mask).

5. SYSTEM CALIBRATION

As in any computational sensing system, we must accurately calibrate the system parameters of our multi-spectral ME imager. In particular, we must characterize the absolute location of the code features and wavelength-dependent shift due to the prism in the coded detector. To accomplish this, we first remove the coded aperture and set the camera's temperature to -30°C to reduce the dark noise. We then place in the optical path a single bandpass filter centered at the wavelengths of interest (using, for example, Thorlabs FB450-40, FB550-40 or FB650-40) and record the light intensity at the camera. Using the SLMs to vary the intensity of a particular spectral channel, we acquire 10 images at maximum (I) and minimum (BG) intensity. We then repeat this experiment with the coded aperture in place to get the coded maximum and background intensities, I_M and BG_M , respectively. We define the calibrated mask as $M(\lambda) = \text{mean}(I_M - BG_M) / \text{mean}(I - BG)$. The exposure time for each spectral channel is on the order of 30 seconds and results in images with a signal to noise ratio (SNR) of approximately 30. This calibration is performed offline and was only done once for all reported experiments.

In order to calibrate the system for measurements with very high spectral resolution (in particular, for the case of a spectrally contiguous object), we introduce an additional procedure. Rather than using only bandpass filters (as described above),

we instead use a tunable monochromator to finely explore the system spectral response over an arbitrary range. We use the Thorlabs OSL1 Fiber illuminator as the calibration light source, which has a power of 150 Watts and a visible spectrum from 300 nm to 800 nm. A liquid light guide (LLG0338-6), which connects the light source and the monochromator, transmits the light into the monochromator (Horiba iHR-320). By adjusting the position of the grating inside the monochromator, a certain output wavelength can be selected. The bandwidth of the output light can be controlled by changing the width of the input and output slit. By setting both the input and output slit width to the smallest value of 0.8 mm, the output bandwidth becomes 1.8 nm (the narrowest that we can achieve). We illuminate the diffuser with the output light from the monochromator through another liquid light guide. By scanning through our contiguous spectral range of interest (here we use 60 nm) with a step size of 1 nm, we obtain 60 coded images corresponding to 60 different wavelengths. Each measurement takes an exposure time of only two seconds. We then repeat the same procedure to measure the uncoded images and background images, with the result that we obtain 60 images of the wavelength-dependent coded aperture. Fig. S4 (a) shows the spectrum of the bandpass filters used in the contiguous experiment along with the high-resolution monochromator channels. To reconstruct the object onto a user-defined set of spectral channels (both in terms of location and width), we can combine the 60 calibration channels to determine the coded detector response for those channels. For example, combining every 10 monochromator bins allows for reconstruction onto six spectral channels with an average bandwidth of 10 nm, as shown in Fig. S4 (b). The image of the coded aperture of the new (combined) channel can be obtained by simply averaging the coded aperture image of all subchannels inside it.

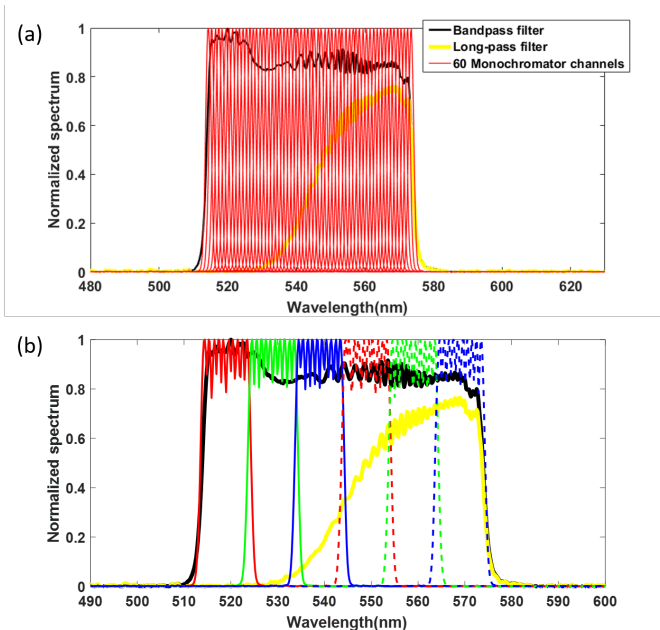


Fig. S4. Spectrum plots in calibration (a) Spectrum of the bandpass and longpass filters that modulate the object and spectrum of the 60 calibration channels. (b) Spectrum of the bandpass and longpass filters that modulate the object and spectrum of the six, binned calibration channels.

6. RECONSTRUCTION ALGORITHM

Our approach to recovering (i.e. demultiplexing) speckle from the individual spectral channels and, subsequently, processing the distinct speckle patterns to recover the multi-spectral object involves the combination of several well-established algorithms. We first recover the speckle by learning a basis that is matched to the spatial structure present in speckle patterns and enforcing sparsity in this “speckle” basis. We then perform traditional correlation-based ME processing through a combination of phase retrieval and/or bispectrum analysis. To provide additional insight into this process, we describe the motivation and implementation of each of these approaches.

As described by Llull et al. [1], a pixel-wise spectral coding scheme can be formulated in terms of a linear forward model. The coded, multiplexed measurement $I(x,y)$ can be written as

$$I(x,y) = \sum_{\lambda} T_{\lambda}(x,y) \cdot I_{\lambda}(x,y) \quad (S1)$$

This forward model can be rewritten in a matrix form:

$$Y = HX,$$

which is an under-determined linear system, and can be solved under some sparse basis D_c :

$$Y = HD_c\alpha.$$

The choice of reconstruction algorithm (including the associated priors and choice of sparse representation) also impacts the system performance. For example, we have explored the Generalized Alternating Projection [2] algorithm, which uses a wavelet basis as a sparse representation of the speckle; however, because speckle is not a natural image, this basis failed to match the data and the observed performance was poor. We have also explored algorithms based on minimizing the Total Variation of the signal[3]; however since the raw speckle measurement has an incredibly low image contrast, the performance is also limited. As a dictionary learning approach is able to accurately reflect the structure of the speckle pattern, we use an algorithm called beta process factor analysis (BFPA[4]) to learn the sparse basis D_c . Once D_c was learned, we use the orthogonal matching pursuit (OMP) algorithm to solve for the α . BFPA combined with OMP results in significantly improved performance with both the experimental and emulated data relative to the previously-mentioned approaches. Once we recover the speckle associated with each spectral channel, we follow the methods of Bertolotti et al. [5] and Katz et al. [6] and perform our choice of phase retrieval algorithm (in this work we choose conjugate gradient descent, but any comparable method can suffice [7]).

7. ISSUES ARISING FROM AUTOCORRELATION IMAGING

There are a number of issues that arise in the context of autocorrelation-based imaging methods and are not unique to this work. However, these issues do pose additional challenges in the context of our proposed method, specifically with regard to the fusion of the object recovered in the individual channels into a comprehensive estimate of the spatio-spectral object. Below we briefly detail these issues and general strategies that can be applied in order to address them.

A. The twin-image problem

Conventional phase retrieval algorithms, when solving for an object with a given autocorrelation function, will return inverted versions of the object (flipped in x and y) 50% of the time, as the phase information that resolves this ambiguity is not recoverable from autocorrelation processing. The solution is to use instead process the recorded speckle data using bispectrum processing (e.g. [8]) which recovers the absolute phase of the object up to an overall phase gradient. The recovered object from bispectrum processing can then be used as an initial-guess in further runs of an iterative phase retrieval algorithm to further refine the result. Given the bispectrum as the initial guess, the estimated object will always have the proper orientation.

B. Ambiguity in absolute object location

In conventional phase retrieval and bispectrum processing, the recovered phase is ambiguous to within an overall gradient—corresponding to a shift of the recovered object. This means the relative position of the recovered objects in the different spectral channels must be first be determined in order to form a comprehensive estimate of the full spatio-spectral object. There are a number of approaches that can potentially help with the task of co-registration.

First, if there exists spatial correlations between the object appearance in different spectral bands, cross-correlation of the recovered objects in the different channels can be used to extract and estimate of the relative shift that should be applied to co-register the channels. This is the method that was used in this manuscript. Note that the presence of these correlations does not imply that there is correlation in the speckle in these channels (the channels can be separated by more than the spectral correlation length of the speckle). Note also that the correlation in object structure need not exist across all channels—only that correlations between groups of channels exist that span and link the full set of channels.

Second, if the spectral channels are separated by less than the spectral correlation length, the individual speckle measurements can be cross-correlated to extract estimates of the relative shifts of the object structures in the channels. Again, this does not require that all channels fall within a single spectral correlation length, only that each channel is within a chain of correlations that allow it to be referenced within the overall set.

Finally, note that these strategies do not cover all possible cases, and there are scenarios for which they will fail (e.g. widely-separated spectral channels with spatial structure that is fully uncorrelated from one channel to another) and under which the recovered spectral channels cannot be unambiguously co-registered. We are currently investigating whether multi-measurement approaches based upon strategies such as the transport of intensity equation (TIE) or ptychography can be modified to resolve the shift ambiguity.

8. SPECTRAL RESOLUTION ANALYSIS

The spectral resolution of the hyperspectral imager is determined by both the design of hardware (spacing, dispersive element, relay lens and the camera pitch size) as well as the reconstruction scheme (choice of reconstruction algorithm and the compression ratio $1/N_\lambda$). The coded patterns of two adjacent but distinct wavelengths can potentially fall on the camera with a spatial separation less than 1 pixel. As indicated by other authors [9] the patterns need to be separated by the order of 1 detector pixel to be accurately de-multiplexed (although we find

that we can outperform this metric). In this section, we analyze the spectral resolution of our system by emulation, using the 60 coded masks calibrated with a monochromator.

The separation between spectral channels on the camera is determined by separation of the central wavelength (CWL) of each channel. In this analysis, we assume that all channels have equal bandwidths; therefore, we investigate the image quality of the recovered speckles as a function of the average separation between the reconstruction channels (i.e., mean difference of the contiguous channels over the full bandwidth). For the case of $N_\lambda = 6$, we use every k calibration channels to formulate one reconstruction channel. Since the spectral difference between 2 adjacent calibration channels is 1 nm, the mean difference of the adjacent CWL across the 6 reconstruction channels is k nm. We first obtain the mask of each reconstruction channel by averaging the masks of the k corresponding calibration channels, then we emulate the single shot compressed measurement by multiplexing the mask of each reconstruction channel with an un-coded speckle pattern and sum all the coded speckle patterns. Finally, we perform the reconstruction and compute the average correlation coefficient of the 6 recovered speckles. We repeat the analysis procedure for $N_\lambda = 2$ case, which corresponds to fewer channels and, correspondingly, simpler de-multiplexing. //

The results of both cases are plotted in Fig. S5 (a). For $N_\lambda = 6$, we find that the quality of the recovered speckles are good until the separation falls below 5 nm. This is because the coded speckles are not separated wide enough on the sensor (only 0.15 pixels, as indicated in Fig. S5 (b)), which causes the demultiplexing algorithm to gracefully fail. While a larger separation improves performance, it never approaches the recovered speckle quality of the $N_\lambda = 2$ case. For this latter case, the resolution is on the order of 4-5 nm, but the overall performance is better due to the fact that the degree of multiplexing is reduced. Note, however, that the resolution will depend both on the number of channels as well as choice of object

9. SPATIO-SPECTRAL COMPLEXITY

In Ref.[6], the notion of object “complexity” was defined as the number of individual resolution elements that compose the object. In this context, object complexity was a qualitative stand-in for the difficulty of object recovery via ME imaging, given that the nonlinear processing renders performance object-dependent. From a computational sensing perspective, one can interpret the role of the complexity metric as identifying how many speckle patterns corresponding to individual object points are multiplexed together in the final measurement. As multiplexing of this type increases, the information about the object is compressed into small variations on a large baseline and dynamic range and SNR issues than come into play in determining how easily the resulting measurements can be inverted to recover the object. Using this intuitive understanding of the role of object complexity, we can then make the obvious generalization for the spatio-spectral case. The complexity of an object with spatio-spectral structure is the number of individual resolution elements in the object *spectral datacube* that compose the object. For example, the complexity of the numbers in Fig. 3 is 3177, the cell from the stem of a cotton plant is 3312, and the letter “H” in Fig. 4 is approximately 2700, which indicates the relative difficulty in imaging these objects.

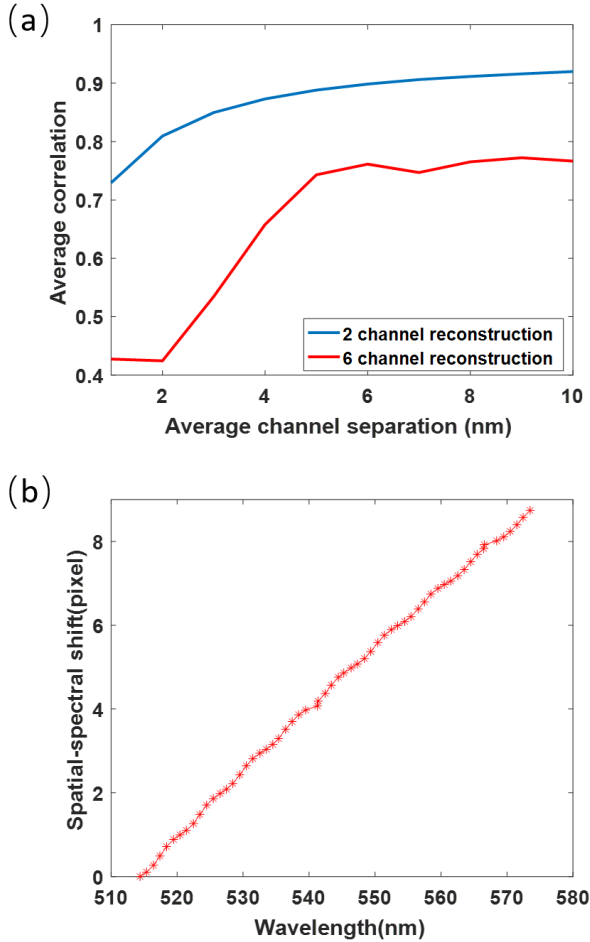


Fig. S5. Data acquisition and reconstruction pipeline. (a) Reconstruction performance as a function of average channel separation. $N_\lambda = 2$ has an overall better performance than $N_\lambda = 6$ case because of a reduced multiplexing penalty. When the channels are separated by more than 5 nm, the performance is limited only by multiplexing penalty. We identify this shoulder as indicative of the spectral resolution of the system. (b) Spatial-spectral shift of the 60 calibration channels.

REFERENCES

1. P. Llull, X. Liao, X. Yuan, J. Yang, D. Kittle, L. Carin, G. Sapiro, and D. J. Brady, "Coded aperture compressive temporal imaging," *Opt. Express* **21**, 10526–10545 (2013).
2. X. Liao, H. Li, and L. Carin, "Generalized alternating projection for weighted- ℓ_2, ℓ_1 minimization with applications to model-based compressive sensing," *SIAM J. Imag. Sci.* **7**, 797–823 (2014).
3. H. Y. H. Huang, L. Tian, Z. Zhang, Y. Liu, Z. Chen, and G. Barbastathis, "Path-independent phase unwrapping using phase gradient and total-variation (tv) denoising," *Opt. Express* **20**, 14075–14089 (2012).
4. M. Zhou, H. Chen, J. Paisley, L. Ren, L. Li, Z. Xing, D. Dunson, G. Sapiro, and L. Carin, "Nonparametric bayesian dictionary learning for analysis of noisy and incomplete images," *IEEE Transactions on Image Process.* **21**, 130–144 (2012).
5. J. Bertolotti, E. G. van Putten, C. Blum, A. Lagendijk, W. L. Vos, and A. P. Mosk, "Non-invasive imaging through opaque scattering layers," *Nature* **491**, 232–234 (2012).
6. O. Katz, E. Small, and Y. Silberberg, "Looking around corners and through thin turbid layers in real time with scattered incoherent light," *Nat Photonics* **6**, 549–553 (2012).
7. J. R. Fienup, "Phase retrieval algorithms: a comparison," *Appl. Opt.* **21**, 2758–2769 (1982).
8. T. Wu, O. Katz, X. Shao, and S. Gigan, "Single-shot diffraction-limited imaging through scattering layers via bispectrum analysis," *Opt. Lett.* **41**, 5003–5006 (2016).
9. G. Arce, D. Brady, L. Carin, H. Arguello, and D. S. Kittle, "Compressive coded aperture spectral imaging," *IEEE Signal Process. Mag.* **31**, 105–115 (2014).